

# Null-space-based path-following control for cooperative payload transport using multiple rotorcraft UAVs

Lucio R. Salinas, Javier Gimenez, Claudio Rosales and Daniel C. Gandolfo

**Abstract**—This paper considers the problem of carrying a payload hanging through flexible cables from rotorcraft unmanned aerial vehicles (RUAVs), taking into account obstacle avoidance, even distribution of payload weight between the aircrafts, and formation shape. The simultaneous fulfillment of these objectives, prioritizing obstacle avoidance, is achieved by using a null-space-based control. In this approach the payload must follow a predetermined path to avoid possible oscillations. In addition, an accurate 6-DoF nonlinear dynamic model of a mini-helicopter and dynamic models for the cables and payload are included to consider a realistic scenario. Finally, simulation results show the good performance of the proposed approach.

## I. INTRODUCTION

Today, there is a large interest worldwide in the development of RUAVs for several civil and military missions due to its fully demonstrated utility including cost reduction and its high mobility in a three-dimensional space (capacities to move in all directions, fly at low speed, take off and land vertically in small spaces and hover). Aerial transportation using RUAVs is a new interesting solution in many transport applications. However, this is a challenging and hazardous task since the load changes significantly the flight characteristics of the aerial vehicles.

In the literature, numerous control techniques have been proposed for different application in aerial transportation. The authors in [1] propose modeling the system of a RUAV carrying a cable-suspended payload as a hybrid dynamical system, designing maneuvers that not only produce large load swings, but also periods where the cable connection between the load and the RUAV is not present. Then, a nonlinear controller to control a RUAV with-load states is reported with satisfactory experimental results. In order to deal with the problem to transport and manipulate loads safely and efficiently, in [2] it is proposed an adaptive controller considering changes in the center of gravity and optimal trajectory generation based on dynamic programming for swing-free maneuvering. In similar way, a geometric nonlinear control of a RUAV transporting and delivering a payload connected via a length-varying cable is presented in [3]. In this proposal, the RUAV transports the payload to a desired position avoiding oscillations by keeping the load in the vertical plane that contains its flight direction. To deal with the problem of lifting from the ground a cable-suspended load by a RUAV, the authors in [4] and [5] break down the lift maneuver

L.R. Salinas, J. Gimenez, C. Rosales and D.C. Gandolfo are with the Instituto de Automática (INAUT), Universidad Nacional de San Juan, CONICET, San Juan, Argentina  
{lsalinas,jgimenez,crosales,dgandolfo}@inaut.unsj.edu.ar

into simpler modes which represent the dynamics of the RUAV-load system at particular operating regimes and obtain waypoints to be reached by the aerial vehicle to accomplish the task. After that, an adaptive controller that follows a desired trajectory based on waypoints is presented and validated by numerical simulations and experimental results. On the other hand, an interesting approach is presented in [6], in which the flexible cable is modeled as a system of serially-connected links and has been considered in the full dynamic model. Then, a nonlinear control system is used in order to exponentially stabilize the position of the RUAV while aligning the links to the vertical direction below the RUAV. All these approaches are interesting, but only one UAV is used in the load transportation [7], [8], [9], [10].

The load stability and the load capacity can be improved by increasing the number of RUAVs. Multi-Vehicle version of the problem is a hard issue due to the suspended payload produce load-RUAV and RUAV-RUAV perturbations. Many authors have considered the aerial load transportation using two RUAVs with satisfactory results [11], [12]. In [13] it is proposed outdoor field experiments of transportation and deployment of loads with single/multiple RUAVs, highlighting the motivation for using two or more small helicopters instead of one with bigger load capacity. In this context, developments with both flexible cables [14], [6], [15] and rigid links [16] have been reported in last years. In all these cases nonlinear controllers are proposed for the payload follows a desired trajectory demonstrating the good performance via simulation and experimental results. The authors in [17] develop a complete dynamic model of a payload viewed as a rigid body with point mass. Then, a feasible trajectory for the payload+RUAVs system is dynamically found by using the differential flatness property. The cooperation and control of multiple aerial robots with sensing and actuation capabilities for the deployment of loads is addressed in [18] using a AWARE multi-UAV platform. In this approach, the general scheme of the proposed control algorithm for one or several helicopters coupled with the load is composed of two loops: the outer loop for translation control and inner loop to control the orientation of each helicopter. Experimental results with three helicopters show the good performance of the proposal. In the addressed literature all control approaches are interesting, however they do not consider obstacle avoidance (that may unexpected appear along the desired path). In addition, in transportation through aerial vehicles, is vitally important to ensure the even distribution of load weight between the RUAVs that make up the formation, as well as being able

to choose the geometric shape of the such formation. The aforementioned works do not consider these situations.

In this paper we propose a multi-vehicle cooperative path-following control, based on mathematical theory of null-space. In this approach, a payload follows a desired path, considering obstacle avoidance, even distribution of the payload weight between the RUAVs and the possibility of choosing the geometric shape of the formation. The control objectives are achieved in a priority order without generating conflicts between them. Since this is a kinematic control approach, the outputs of the proposed kinematic controller are coupled with a dynamic model of any RUAV through an adaptation stage to obtain the control actions necessary to reach the kinematic references. In this paper, a very accurate dynamic model of a mini-helicopter [19] and a model for the load and flexible cables are considered to evaluate and validate the control strategy in a real test scenario.

## II. PROBLEM FORMULATION

Consider  $n$  RUAVs cooperatively carrying a cable-suspended payload. Each vehicle has position  $\xi_i = [x_i, y_i, z_i]^T$ , which coincides with its gravity center (g.c.), and orientation  $\psi_i$ . In this paper, the system configuration is given by  $\mathbf{q} = [\xi_1^T, \psi_1, \dots, \xi_n^T, \psi_n]^T$ . In addition, consider a point-mass payload jointed to each vehicle with cables of length  $\ell$ .

The formation must fulfill a number of tasks sorted according to predetermined priorities establishing which one of them can be omitted in critical situations. Obstacles avoidance is the highest priority task in this paper, and for this, a 3D-laser is incorporated to each vehicle. The secondary objectives are: the load weight should be properly distributed between the vehicles; the vehicle positions must conform a pre-set shape; the payload must follow a predetermined path reducing oscillations caused by external factors such as wind; and each vehicle must be oriented according to a desired path-dependant angle. The payload weight can be evenly distributed among the vehicles according to different factors such as lift capacity or limited on-board energy. All these tasks can be performed simultaneously only when there are no obstacles nearby.

Based on null-space theory, this paper proposes kinematic velocities  $\mathbf{v}_c$  for the configuration variable  $\mathbf{q}$  necessary to fulfill as many tasks as possible, and subsequently, the control actions necessary to reach these velocities are provided in an external loop.

## III. TASK VARIABLES AND THEIR JACOBIANS

Task variables are quantities that characterize directly the tasks to be fulfilled, and whose derivatives are linearly related to  $\dot{\mathbf{q}}$  through Jacobians. The relation between configuration and task variables allows a straightforward definition of the kinematic controller  $\mathbf{v}_c$ . This section presents the task variables and their respective Jacobians, which are classified in four groups: formation, payload, distance and orientation variables.

### A. Formation variables

The formation state is characterized by the relative positions of the vehicles, which is defined by

$$\xi_{r,i} := \begin{bmatrix} \xi_{r,i,x} \\ \xi_{r,i,y} \\ \xi_{r,i,z} \end{bmatrix} := \xi_i - \bar{\xi},$$

where

$$\bar{\xi} := \frac{1}{n} \sum_{i=1}^n \xi_i,$$

is the mean position. Their time derivatives are given by

$$\dot{\xi}_{r,i} = \mathbf{J}_{r,i} \dot{\mathbf{q}}, \quad (1)$$

where

$$\mathbf{J}_{r,i} := \begin{bmatrix} \mathbf{J}_{r,i,x} \\ \mathbf{J}_{r,i,y} \\ \mathbf{J}_{r,i,z} \end{bmatrix} = [\Delta_{i1} \ \Delta_{i2} \ \dots \ \Delta_{in}],$$

with

$$\Delta_{ij} := \begin{cases} -\frac{1}{n}\Delta & \text{if } i \neq j \\ \frac{n-1}{n}\Delta & \text{if } i = j \end{cases}, \quad \Delta := \begin{bmatrix} 1 & 0 & 0 & 0 \\ 0 & 1 & 0 & 0 \\ 0 & 0 & 1 & 0 \end{bmatrix}.$$

Rewriting equation (1) into matrix form,

$$\dot{\xi}_r = \mathbf{J}_r \dot{\mathbf{q}}, \quad (2)$$

where

$$\dot{\xi}_r := \begin{bmatrix} \dot{\xi}_{r,1} \\ \vdots \\ \dot{\xi}_{r,n} \end{bmatrix}, \quad \text{and} \quad \mathbf{J}_r := \begin{bmatrix} \mathbf{J}_{r,1} \\ \vdots \\ \mathbf{J}_{r,n} \end{bmatrix}.$$

### B. Payload variables

The payload position  $\xi_\ell = [x_\ell, y_\ell, z_\ell]^T$  is another variable of interest, which is given by

$$\xi_\ell := \bar{\xi} - \mathbf{h},$$

where  $\mathbf{h} = \mathbf{h}(t) = [\mathbf{h}_x(t), \mathbf{h}_y(t), \mathbf{h}_z(t)]^T$  is the relative position of the payload respect to the mean position. The time variation of  $\mathbf{h}$  is mainly caused by payload oscillations. The payload velocity is given by

$$\dot{\xi}_\ell = \mathbf{J}_\ell \dot{\mathbf{q}} - \dot{\mathbf{h}}, \quad (3)$$

where

$$\mathbf{J}_\ell := \begin{bmatrix} \mathbf{J}_{\ell,x} \\ \mathbf{J}_{\ell,y} \\ \mathbf{J}_{\ell,z} \end{bmatrix} := \frac{1}{n} [\Delta \ \Delta \ \dots \ \Delta].$$

### C. Distance variables

The  $x$ - $y$  distances  $d_{i,j} := \|\xi_{i,xy} - \xi_{j,xy}\|$ ,  $i < j$ ,  $\xi_{i,xy} = [\xi_{i,x}, \xi_{i,y}]^T$ , between vehicles should be considered in order to avoid internal collisions. The respective Jacobians are given by

$$\dot{d}_{i,j} = \frac{(\xi_{i,xy} - \xi_{j,xy})^T (\dot{\xi}_{i,xy} - \dot{\xi}_{j,xy})}{d_{i,j}} = \mathbf{J}_{d,i,j} \dot{\mathbf{q}}, \quad (4)$$

where

$$\begin{aligned} \mathbf{J}_{d,i,j} &= \mathbf{J}_{d,i,j}(\mathbf{q}) = \frac{1}{d_{i,j}} (\xi_{i,xy} - \xi_{j,xy})^T \\ &\times [\mathbf{0}_{2 \times 4(i-1)}, \mathbf{I}_2, \mathbf{0}_{2 \times 4(j-i-1)+2}, -\mathbf{I}_2, \mathbf{0}_{2 \times 4(n-j)+2}], \end{aligned}$$

with  $\mathbf{I}_2$  denoting the  $2 \times 2$  identity matrix.

Rewriting equation (4) into matrix form,

$$\dot{\mathbf{d}} = \mathbf{J}_d \dot{\mathbf{q}}, \quad (5)$$

where

$$\mathbf{d} := [d_{i,j}]_{i < j} = \begin{bmatrix} d_{1,2} \\ \vdots \\ d_{n-1,n} \end{bmatrix}, \quad \mathbf{J}_d := [\mathbf{J}_{d,i,j}]_{i < j} = \begin{bmatrix} \mathbf{J}_{d,1,2} \\ \vdots \\ \mathbf{J}_{d,n-1,n} \end{bmatrix}.$$

### D. Orientation variables

Finally, the orientation variables are the vehicle orientations  $\psi_i$ , whose associated Jacobians are given by

$$\mathbf{J}_{\psi_i} := [\delta_{i1} \quad \delta_{i2} \quad \cdots \quad \delta_{in}],$$

where

$$\delta_{ij} := \begin{cases} [0 \quad 0 \quad 0 \quad 1] & \text{if } i = j, \\ [0 \quad 0 \quad 0 \quad 0] & \text{if } i \neq j. \end{cases}$$

Then

$$\dot{\psi} = \mathbf{J}_{\psi} \dot{\mathbf{q}}, \quad (6)$$

where

$$\psi := \begin{bmatrix} \psi_1 \\ \vdots \\ \psi_n \end{bmatrix}, \quad \text{and} \quad \mathbf{J}_{\psi} := \begin{bmatrix} \mathbf{J}_{\psi_1} \\ \vdots \\ \mathbf{J}_{\psi_n} \end{bmatrix}.$$

## IV. CONTROL OBJECTIVES

### A. Distribution of the payload weight

The payload weight produces a force  $F_i$  with norm  $f_i$  on each vehicle (see Fig. 2). These forces are noisy by nature, so, in order to generate smooth control actions, a low-pass filter (moving average) is applied to each signal obtaining  $\check{f}_i$ , these are then incorporated in the control loop.

When all the vehicles navigate at the same altitude, the vehicles in the back of the formation perform less effort. Each vehicle can regulate its effort by modifying its altitude, since the higher it is  $\xi_{r,i,z}$  the greater is the payload weight proportion that it bears. Consider that the payload weight proportion for each vehicle is respectively set in  $\rho_i$ , with  $\sum_{i=1}^n \rho_i = 1$ . Then, the desired relative altitude for each vehicle in order to bear the desired weight is given by

$$\xi_{r,i,z}^* := \xi_{r,i,z} - k_{w,1} \tanh \left( k_{w,2} \left( \frac{\check{f}_i}{\rho_i} - \sum_{j=1}^n \check{f}_j \right) \right), \quad (7)$$

with  $k_{w,1}, k_{w,2} > 0$ . Then, the control objective is  $\tilde{\xi}_{r,i,z}(t) := \xi_{r,i,z}^*(t) - \xi_{r,i,z}(t) \rightarrow 0$ . Note that each  $\rho_i$  can vary in time according to the on-board energy or other factors.

### B. Formation

To define the desired formation, only the relative positions  $\xi_{r,i}^* = [\xi_{r,i,x}^*, \xi_{r,i,y}^*, \xi_{r,i,z}^*]^T$  desired for each vehicle must be specified, which can be time variant. The desired relative altitudes  $\xi_{r,i,z}^*$  were defined in (7) for load weight distribution, and thus, only  $\xi_{r,i,xy}^* = [\xi_{r,i,x}^*, \xi_{r,i,y}^*]^T$  can be set in order to define a desired formation. Then, the formation objective control is  $\tilde{\xi}_{r,i,xy}(t) := \xi_{r,i,xy}^*(t) - \xi_{r,i,xy}(t) \rightarrow 0 \forall i$ .

### C. Path following

The payload oscillations can be reduced by requiring that the payload follows a path  $\xi^*(s) = [x^*(s), y^*(s), z^*(s)]^T$  parameterized by arc length. This path can be characterized by the orientations given by

$$\psi^*(s) := \text{atan2} \left( \frac{\partial \xi^*}{\partial y^*}(s), \frac{\partial \xi^*}{\partial x^*}(s) \right),$$

and

$$\theta^*(s) := \text{atan2} \left( \frac{\partial \xi^*}{\partial z^*}(s), \sqrt{\left( \frac{\partial \xi^*}{\partial x^*}(s) \right)^2 + \left( \frac{\partial \xi^*}{\partial y^*}(s) \right)^2} \right).$$

There is a function  $s = s(t)$  such that

$$s(t) := \arg \min_s \|\xi_\ell(t) - \xi^*(s)\|.$$

This is,  $\xi^*(s(t))$  is the point on the curve  $\xi^*(s)$  closest to  $\xi_\ell(t)$  at each time  $t$ . Then,  $\psi^*$  and  $\theta^*$  are also functions of  $t$ .

Given a desired flight velocity for the payload

$$\nu^* = \nu^*(t) := \frac{\nu_{max}^*}{1 + k_{\ell,1} \tanh(k_{\ell,2} \|\xi_\ell(t) - \xi^*(s(t))\|)}, \quad (8)$$

with  $k_\ell > 0$  and maximum desired velocity  $\nu_{max}^* > 0$ , the control objective is  $\|\xi_\ell(t) - \xi^*(s(t))\| \rightarrow 0$ .

### D. Vehicle orientations

The desired vehicle orientations  $\psi^*(s(t))$  is selected tangent to the path at  $\xi^*(s(t))$  to take advantage of the benefits of forward flight in some RUAVs like mini-helicopters. Then, the control objective is that  $\psi_i(t) - \psi^*(s(t)) \rightarrow 0 \forall i$ .

### E. Obstacle avoidance

There are two types of obstacles to be considered: internal and external. For each vehicle, the other vehicles and the payload are internal obstacles. On the other hand, out-of-formation objects are considered external obstacles.

It is supposed that the load-vehicle collisions are avoided by considering  $\rho_i > 0$ . The collisions between vehicles are avoided by defining a minimal desired distance  $d_{min} > 0$  for which the control objectives are that  $d_{ij} > d_{min} \forall i, j$ .

Because the vehicles are linked through the payload, the avoidance of external obstacles must be joint and cooperative. The modification of the reference path and the desired

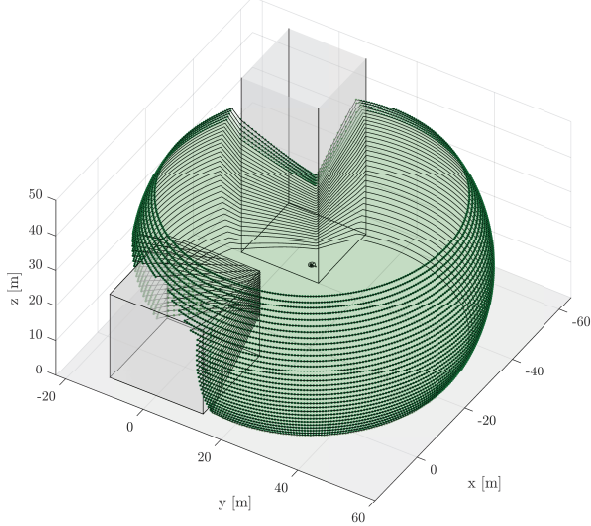


Fig. 1. Paths traced by a 3D LiDAR sensor on board the mini-helicopter. The LiDAR has  $360^\circ$  and  $\pm 30^\circ$  horizontal and vertical FOV, respectively, and 40 meters range.

relative positions are the alternative chosen in this paper to avoid obstacles. These modifications are based on sensors readings obtained with a 3D LiDAR sensor on board each vehicle.

Every LiDAR observation generates a fictitious force using the following expression

$$FF_i = \begin{bmatrix} F_{lon,i} \\ F_{lat,i} \\ F_{ver,i} \end{bmatrix} = \begin{bmatrix} k_{lon} \sum_{k=1}^m D_k \cos \vartheta_k \cos \varphi_k \\ k_{lat} \sum_{k=1}^m D_k \sin \vartheta_k \cos \varphi_k \\ k_{ver} \sum_{k=1}^m D_k \sin \varphi_k \end{bmatrix}, \quad (9)$$

being  $F_{lon,i}$ ,  $F_{lat,i}$  and  $F_{ver,i}$  the longitudinal, lateral and vertical fictitious forces of vehicle  $i$ , respectively. Constants  $k_{lon}$ ,  $k_{lat}$  and  $k_{ver}$  are used to normalize forces.  $D_k = a - bd_k(t)$  indicates the magnitude of the force for each laser beam ( $1 \leq k \leq m$ ), with  $a, b > 0$  such that  $a - bD_{max} = 0$  and  $a - bD_{min} = 1$  for  $D_{min} \leq d_k \leq D_{max}$ <sup>1</sup>. The angles  $\vartheta_k$  and  $\varphi_k$  express the direction of each laser beam in the horizontal and vertical plane respectively. See Fig. 1 for a graphical representation of a  $360^\circ$  and  $\pm 30^\circ$  horizontal and vertical FOV LiDAR, respectively.

For simplicity, each sensor is simulated as a gimbaled LiDAR, hence,  $F_{ver,i}$  coincides with global z-axis. Then,  $FF_i$  is rotated using  $\psi_i$  to express the fictitious force in global coordinates<sup>2</sup> as  $\varsigma_i = R(\psi_i)FF_i$ .

The mean fictitious force,  $\bar{\varsigma} := \frac{1}{n} \sum_{i=1}^n \varsigma_i$ , is used to modify the path reference through the following formula

$$\xi_{new}^* = \xi^*(s(t))_{new} := \xi^*(s(t)) + \mathbf{K}_{\xi,1} \tanh(\mathbf{K}_{\xi,2} \bar{\varsigma}), \quad (10)$$

where  $\mathbf{K}_{\xi,1}$ ,  $\mathbf{K}_{\xi,2}$  are design matrices. Note that  $\tanh$  is used as a component-wise vector function.

<sup>1</sup>The distance  $D_{min}$  can be set to avoid occlusion with the formation ignoring any reading below this value.

<sup>2</sup>If the LiDAR is not placed on a gimbal, then forces  $F_{lon,i}$ ,  $F_{lat,i}$  and  $F_{ver,i}$  must be filtered and the rotation matrix must include the vehicle's roll and pitch angles to properly obtain  $\varsigma_i$ .

Simultaneously, each vehicle can use  $\varsigma_i$  to modify its desired relative position in the formation incorporating flexibility when necessary. The change in the relative position is made through the following formula

$$\xi_{r,i,xy,new}^* = \xi_{r,i,xy,new}^*(t) := \xi_{r,i,xy}^*(t) + \mathbf{K}_{\xi_r} \varsigma_{i,xy}, \quad (11)$$

only if  $\xi_{i,xy}^T \xi_{r,i,xy} < 0$ , i.e., if the relative position of the vehicle is modified in the direction of  $\bar{\xi}$ , avoiding an undesired reshape of the formation.  $\mathbf{K}_{\xi_r}$  is a design matrix

Note that the frontal component of  $FF_i$  ( $F_{lon,i}$ ) is discarded and not used in the modification of the reference path, although it can be incorporated to appropriately reduce  $\nu^*$ .

## V. CONTROLLER BASED ON NULL-SPACE

The kinematic velocities  $\mathbf{v}_c$  of the vector state  $\mathbf{q}$  required to fulfill the predefined tasks and their priorities are found in this Section. A controller based on null-space [20] is used to this end. This controller has a geometric deduction and works projecting desired velocities of lower priority tasks on the null-space of the Jacobian of the higher priority tasks.

There is a conflict between tasks when they can not be simultaneously verified. The definition of the task variables, the priorities between tasks, and the control objectives are key issues to avoid as many conflicts between tasks as possible. The under-actuated characteristic of the multi-robot system requires a meticulous and complex definition of these settings.

If the velocity vector  $\mathbf{v}_c^{(1)}$  satisfies the first task (highest priority task or task 1), then the set of desired velocity vectors for which task 1 is verified is conformed by the vectors of the form

$$\mathbf{v} = \mathbf{v}_c^{(1)} + (\mathbf{I}_{4n} - \mathbf{J}_1^\dagger \mathbf{J}_1) \mathbf{w}, \quad \mathbf{w} \in \mathbb{R}^{4n}, \quad (12)$$

where  $\mathbf{J}_1$  is the Jacobian of task 1,  $\mathbf{I}_{4n}$  is the  $4n \times 4n$  identity matrix, and the superscript  $\dagger$  represents the pseudo-inverse matrix. These velocity vectors satisfy task 1, since  $\mathbf{J}_1 \mathbf{v} = \mathbf{J}_1 \mathbf{v}_c^{(1)}$ .

Note that  $(\mathbf{I}_{4n} - \mathbf{J}_1^\dagger \mathbf{J}_1) \mathbf{w}$  is the orthogonal projection of  $\mathbf{w}$  on the null space of  $\mathbf{J}_1$  denoted by  $\mathcal{N}(J_1)$ . The velocity vector  $\mathbf{v}_c^{(2)}$  defined to fulfill the other tasks is projected on  $\mathcal{N}(J_1)$  so as not to compromise the fulfillment of task 1.

If tasks 1 and 2 are compatible ( $\mathbf{J}_2 \mathbf{J}_1^\dagger = \mathbf{0}$ ), then both objectives can be satisfied at once by using

$$\mathbf{v}_c = \mathbf{v}_c^{(1)} + (\mathbf{I}_{4n} - \mathbf{J}_1^\dagger \mathbf{J}_1) \mathbf{v}_c^{(2)}, \quad (13)$$

since  $\mathbf{J}_2 \mathbf{v}_c = \mathbf{J}_2 \mathbf{v}_c^{(2)}$ . If the tasks are not compatible, then task 2 will not be fulfilled, although it will be performed in the best possible way without conditioning task 1. Note that (13) is (12) with  $\mathbf{w} = \mathbf{v}_c^{(2)}$ .

In order to define the proposed kinematic controller, it only remains to define the kinematic controllers  $\mathbf{v}_c^{(i)}$  of (13) that fulfil the specified tasks in the cooperative payload transport problem.

The tasks of the second objective are achieved by using the controller

$$\mathbf{v}_c^{(2)} = \mathbf{J}_2^\dagger \begin{bmatrix} \dot{\xi}_r^* + \mathbf{K}_{r,1} \tanh(\mathbf{K}_{r,2}(\xi_r^* - \xi_r)) \\ \mathbf{v}^* + \mathbf{K}_{\ell,1} \tanh(\mathbf{K}_{\ell,2}(\xi_{new}^* - \xi_\ell)) - \dot{\mathbf{h}} \\ \dot{\psi}^* + \mathbf{K}_{\psi,1} \tanh(\mathbf{K}_{\psi,2}(\psi^* - \psi)) \end{bmatrix}, \quad (14)$$

with  $\mathbf{K}_{r,1}, \mathbf{K}_{r,2}, \mathbf{K}_{\ell,1}, \mathbf{K}_{\ell,2}, \mathbf{K}_{\psi,1}, \mathbf{K}_{\psi,2}$  design matrices,

$$\mathbf{J}_2 := \begin{bmatrix} \mathbf{J}_r \\ \mathbf{J}_\ell \\ \mathbf{J}_\psi \end{bmatrix},$$

the Jacobian of task 2,

$$\mathbf{v}^* = \begin{bmatrix} \nu^* \sin \theta^* \\ \nu^* \cos \theta^* \cos \psi^* \\ \nu^* \cos \theta^* \sin \psi^* \end{bmatrix},$$

the desired velocity vector to follow the path with velocity  $\nu^*$ , and  $\xi_r^* := [\xi_{r,1,x}^*, \xi_{r,1,y}^*, \xi_{r,1,z}^*, \dots, \xi_{r,n,x}^*, \xi_{r,n,y}^*, \xi_{r,n,z}^*]^T$  the desired relative positions.

These tasks can be simultaneously fulfilled without conflicts between them. Then, the avoidance of external obstacles by modifying references is also verified.

It only remains to define the control actions necessary to avoid collisions between vehicles. Thus, for each  $1 \leq i < j \leq n$  the distance errors are defined as

$$\tilde{d}_{ij} := \begin{cases} d_{ij} - d_{min} & \text{if } d_{ij} < d_{min}, \\ 0 & \text{in the other case.} \end{cases}$$

Then, the Jacobian of task 1 is  $\mathbf{J}_1 = \mathbf{J}_d$ , in which the matrices  $\mathbf{J}_{d,i,j}$  are redefined as null when  $d_{ij} \geq d_{min}$  in order to free up null space for the fulfillment of the secondary tasks. So, the security distances are verified using the controller

$$\mathbf{v}_c^{(1)} = \mathbf{J}_1^\dagger \mathbf{K}_d \tilde{\mathbf{d}}, \quad (15)$$

with  $\tilde{\mathbf{d}} := [\tilde{d}_{1,2}, \dots, \tilde{d}_{n-1,n}]^T$  and  $\mathbf{K}_d$  a design matrix.

## VI. SIMULATION TESTBED AND IMPLEMENTATION OF THE KINEMATIC FORMATION CONTROLLER

To test the control proposal in a realistic scenario, different dynamic models are incorporated in a custom software program developed in C++. The aerial vehicles are simulated using 6DoF models of a mini-helicopter (extracted from [19]) and the cables and payload are simulated using point-like masses joined by springs and dampers for the swinging and waving motion and simple 3D solid objects for the drag. Wind and floor collision are also incorporated in the simulation testbed.

In this section, the mini-helicopter and cable models are explained in more detail along with the interconnection between them. Then the implementation of the kinematic formation controller in the simulation is described.

### A. Mini-helicopter dynamic model

The helicopter model used in the simulation is a high-fidelity nonlinear dynamic model of a small-scale helicopter identified in [19]. It adequately represents the mini-helicopter dynamics in both hovering and low-speed flight envelope (up to 20 [m/sec] forward flight). The model considers non-ideal dynamics such as flapping, drag, and actuator dynamics.

The rigid body equations of motion for the helicopter, incorporating the force and torques exerted by the load, are given by the Newton-Euler equations below,

$$\begin{aligned} \dot{u} &= vr - wq - gs\theta + (X_{mr} + X_{fus}) / m, \\ \dot{v} &= wp - ur + gs\phi c\theta + (Y_{mr} + Y_{fus} + Y_{tr} + Y_{vf}) / m, \\ \dot{w} &= uq - vp + gc\phi c\theta + (Z_{mr} + Z_{fus} + Z_{ht} + Z_\ell) / m, \\ \dot{p} &= qr (I_{yy} - I_{zz}) / I_{xx} + (L_{mr} + L_{vf} + L_{tr} + \mathbf{L}_\ell) / I_{xx}, \\ \dot{q} &= pr (I_{zz} - I_{xx}) / I_{yy} + (M_{mr} + M_{ht} + \mathbf{M}_\ell) / I_{yy}, \\ \dot{r} &= pq (I_{xx} - I_{yy}) / I_{zz} + (-Q_e + N_{vf} + N_{tr}) / I_{zz}. \end{aligned} \quad (16)$$

The set of forces and moments acting on the helicopter are organized by components:  $(\cdot)_{mr}$  for the main rotor;  $(\cdot)_{tr}$  for the tail rotor;  $(\cdot)_{fus}$  for the fuselage;  $(\cdot)_{vf}$  for the vertical fin;  $(\cdot)_{ht}$  for the horizontal stabilizer and  $(\cdot)_\ell$  for the load (cable and payload).  $Q_e$  is the torque produced by the engine to counteract the aerodynamic torque on the main rotor blades. Every component is affected by the wind as the airspeed (relative velocity between an object and the air) influences the main and tail rotor thrust and the fuselage, vertical fin and horizontal stabilizer forces (the effect of wind on the load is explained in Section VI-B). For more details on the helicopter model, see [19].

The force  $Z_\ell$  and torques  $L_\ell, M_\ell$  (highlighted in bold font in (16)) are added to the original helicopter model. They are generated by the force exerted by the load ( $F_i$ ) acting on a spherical joint below the helicopter g.c. ( $\xi_i$ ). The force and torques are computed as follows,

$$Z_{\ell,i} = F_{w,i}, \quad L_{\ell,i} = -F_{v,i}l_\ell, \quad M_{\ell,i} = F_{u,i}l_\ell, \quad (17)$$

being  $[F_{u,i}, F_{v,i}, F_{w,i}]^T$  the load force components expressed in the helicopter's body axes and  $l_\ell = 0.2\text{m}$  the cable connection point distance below the g.c. of the helicopter (see Fig. 2).

The helicopter model is controlled through five input commands ( $C_{md}$ ): main rotor collective and cyclic (longitudinal and lateral) blade pitch, tail rotor blade pitch and throttle; the first four inputs control the helicopter movements (up/down, back/forth, left/right, and yaw), while the last input controls the main rotor speed. The connection between these input commands ( $C_{md}$ ) and the kinematic formation control law ( $\mathbf{v}_c$ ) is made via an adaptation stage described in Section VI-C.

In the simulations, the nominal parameters of the helicopter were used which refer to MIT's X-Cell .60 acrobatic helicopter [19].

### B. Flexible cable and payload dynamic models

The cables are modeled as multiple point-like masses joined by springs and dampers (Kelvin-Voigt models) to al-

TABLE I

PARAMETERS OF THE CABLES AND PAYLOAD.

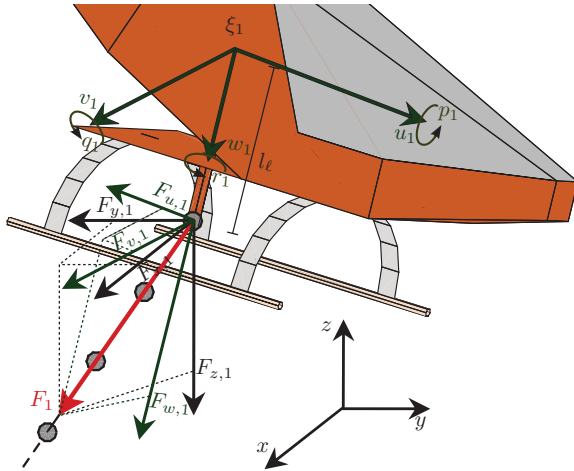


Fig. 2. Graphical representation of the mini-helicopter N°1 and cable connection point (spherical joint) below the helicopter g.c. ( $\xi_1$ ). The load force ( $F_1$ ) is expressed in two coordinate systems: inertial axes  $\langle x, y, z \rangle$  and helicopter's body axes  $\langle u_1, v_1, w_1 \rangle$ .

Parameters	Value
Number of cables	4
Number of masses per cable	39
Cable link mass	0.0033 [kg]
Cable total mass	0.1287 [kg]
Cable diameter	0.004 [m]
Cable drag coefficient	1.0
Payload mass	4.5 [kg]
Payload edge length	0.25 [m]
Payload drag coefficient	1.05
Spring length	0.15 [m]
Spring rate	10000 [N/m]
Spring friction	0.2 [N · s/m]
Gravitational acceleration	9.7917 [m/s <sup>2</sup> ]
Air density	1.151 [kg/m <sup>3</sup> ]
Air friction	0.02 [N · s/m]
Ground repulsion	100 [N/m]
Ground friction	0.2 [N · s/m]
Ground absorption	2 [N · s/m]

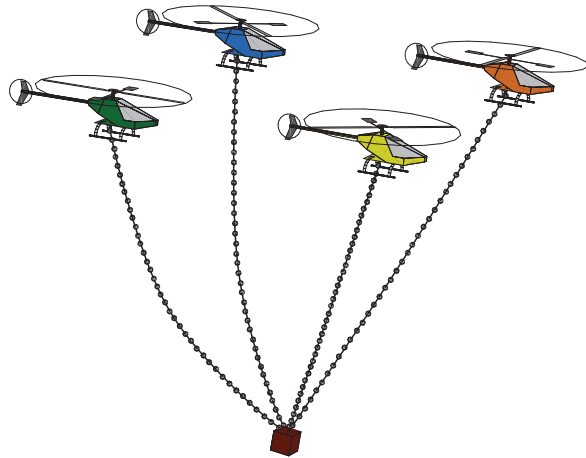


Fig. 3. Graphical representation of mini-helicopters carrying a cable-suspended payload. The cables and payload are simulated using point-like mass particles joined by springs for the swinging and waving motion and simple 3D solid objects for the drag.

low swinging and waving movements. Each cable comprises thirty-nine point-like masses, where the first mass is attached to a spherical joint below the helicopter g.c. (see Fig. 2) and the last mass is connected to a special point-like mass (payload) common to every cable as indicated in Fig. 3. Each mass is affected by the elastic and viscous force generated by the surrounding springs and dampers, the gravitational force, air friction force, drag force and other ground related forces (friction, absorption and repulsion).

The number of links in the cable is set according to the desired detail level; in a six meters cable, the forty links (thirty-nine masses plus payload) give a resolution of fifteen centimeters in the cable's movement. The springs that join each pair of particles (including the payload) are all equal; with a specific length, friction constant and very high rate to avoid excessive stretching of the cable. Others parameters affect the interaction between the cables/payload and the

ground. In addition, the air density and air friction constant are also included in the simulation. The effect of wind on the cable's links and payload are simulated according to the following formula,

$$F_d = \frac{1}{2}\rho v^2 c_d A, \quad (18)$$

where  $\rho$  is the air density,  $v$  is the velocity with respect to air,  $A$  is the cross-sectional area, and  $c_d$  is the drag coefficient. Every link is treated as a solid cylinder and the payload as a solid cube to calculate the cross-sectional area, each with its corresponding drag coefficient<sup>3</sup>. In table I there is a list of all the parameters used in the simulation.

Here is a link to a video showing the dynamic evolution of two mini-helicopters models with flexible cables, such as the ones described in this section, carrying a payload: <http://youtu.be/7kgfY9xIgmc>. Note that wind perturbation as well as payload weight distribution between helicopters ( $f_1$  and  $f_2$  in the video) have been considered.

### C. Implementation of the kinematic formation controller

To let the helicopters track the corresponding flight commands  $\mathbf{v}_{c,i} = [\dot{x}_{i,c}, \dot{y}_{i,c}, \dot{z}_{i,c}, \dot{\psi}_{i,c}]^T$ , the adaptation stage depicted in Fig. 4 is added to each vehicle. This stage is composed by two steps: a velocity frame change and a PID-based cascade control. In the first step, the flight commands  $\mathbf{v}_{c,i}$  are rotated using  $\psi_i$  to align them to a frame attached to the  $i$ -th helicopter, assuming no roll or pitch movements. Then, the PID architecture generates the servo signal inputs  $C_{md,i}$  (see details in [21], [22]).

Fig. 4 exposes the flexibility of this kinematic based controller. Modifying only the adaptation stage it is possible to use the same controller for other types of miniature rotorcraft, e.g., using the PID Adaptation Stage of [23] the kinematic formation controller can be applied to quadrotors.

<sup>3</sup>The cross-sectional area of the payload and cable are considered constant, equal to the cube face area and cylinder lateral area, respectively.

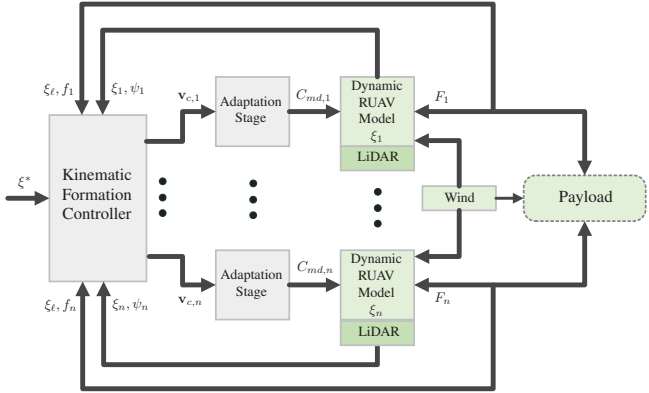


Fig. 4. Simulation testbed and kinematic formation controller framework for  $n$  RUAVs.

The controller is implemented in MATLAB<sup>®</sup> (The MathWorks Inc., Massachusetts, USA) while the adaptation stages and dynamic models are implemented in a custom C++ program<sup>4</sup>; they communicate with each other through shared memory. The formation controller update rate is 60Hz and the adaptation stage update rate is 500Hz. The dynamic models of the mini-helicopters, cables and payload are simulated using a fourth-order Runge-Kutta method with an integration step size of 0.001 seconds.

## VII. SIMULATION RESULTS

In this Section, simulation results are presented to test the controller performance in a realistic simulation environment.

It is well known that following an upward eight-shaped curve is a complicated task. Therefore, to efficiently evaluate the controller performance the reference path chosen to perform the simulation is given by

$$\xi^* = \begin{bmatrix} r \cos(t) \\ r \sin(2t) \\ r \frac{t}{2\pi} + 8 \end{bmatrix},$$

where  $0 \leq t \leq 2\pi$  and  $r = 60$ .

Four mini-helicopters, described in Section VI-A, are simulated carrying a payload of 4.5 kg which hangs from 6 meters long cables. Each cable weights 0.1287 kg, so the total payload weight is approximately 5 kg. This load is evenly distributed between the vehicles ( $\rho_i = 1/4$ ). The desired formation shape is a square of 4 meters. Two obstacles are placed in the simulation environment and a constant wind of 8.5 m/sec (or 19 mph) is incorporated after  $t = 150$  sec. The wind speed corresponds to a “Fresh Breeze” in the Beaufort wind scale, its direction points to the negative x- and y-axis.

Different views of the helicopter formation carrying the payload are shown in Fig. 5, the formation is plotted every 8 sec. The payload path-following error and helicopters formation errors are displayed in Fig. 6, along with the

<sup>4</sup>The cable implementation was inspired by the NeHe OpenGL rope physics tutorial at <http://nehe.gamedev.net>, and the helicopter model is a custom C++ implementation of the equations found in [19].

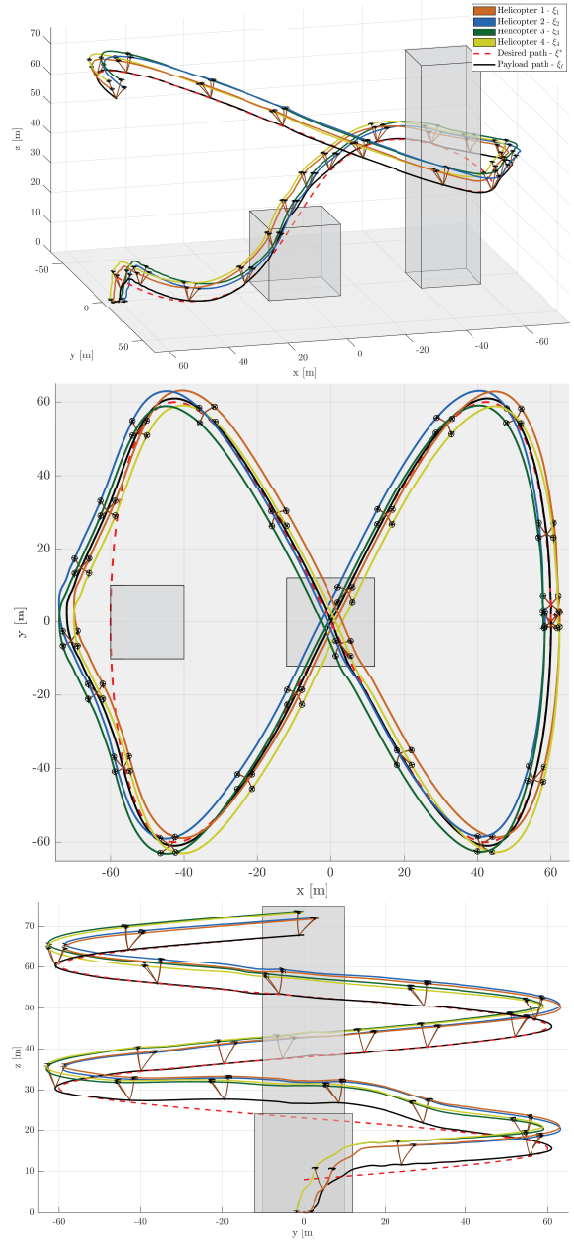


Fig. 5. 3D-view (top), XY-view (middle) and YZ-view (bottom) of the cooperative payload transport simulation, including obstacle avoidance and wind perturbation.

payload weight distribution indicated by the force exerted on each vehicle and the  $xyz$ -velocity commands.

There are two obstacle zones and one wind zone, as depicted in Fig. 6. The first obstacle is easy to surpass increasing the formation altitude, this occurs as a consequence of a path reference change generated by the LiDAR readings (as explained in Section IV-E). The second obstacle is more difficult to avoid, hence the path-following and formation errors increase along with the force produced by the payload. During this avoiding task, the errors increase since these tasks have conflicts with task 1 (see Section V). The  $xyz$ -velocity commands are affected by several factors but mainly by the payload path-following error as indicated in (8).

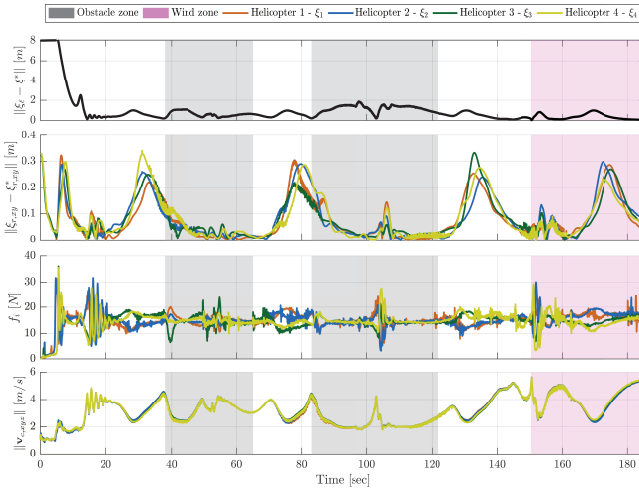


Fig. 6. Payload path-following error (top), helicopters formation errors (second), payload weight distribution (third) and  $xyz$ -velocity commands (bottom) obtained through the cooperative payload transport simulation.

The addition of wind generates an important perturbation in the payload more than in the vehicles because of the size and weight difference. However, the path-following error decreases rapidly.

In general, path-following and formation errors are small except in curves where dynamic effects and the realistic model of the cables introduce oscillations or when the wind suddenly appears.

### VIII. CONCLUSIONS

In this paper, a novel path-following control is proposed in order to carry a payload via flexible cables with multiple rotorcraft UAVs. The control proposal is based on null-space theory considering wind disturbance, obstacle avoidance, as well as properly distribution of the payload weight according to factors such as on-board energy or lift capacity. Accurate dynamic models of a mini-helicopter and a cable-suspended payload are considered to generate a realistic test scenario. The kinematic formation control approach is very flexible since it can be used for another type of aircraft by changing only the adaptation stage.

Figures of the simulation show the good performance of the proposed controller. The tasks were completed according to their pre-established priorities reducing as much as possible the conflicts between them. The incorporation of the mini-helicopter and payload dynamic models in the simulation allows a very fine adjustment of the kinematic controller parameters reducing the gap between simulation and experimentation.

### REFERENCES

- [1] S. Tang, "Aggressive Maneuvering of a Quadrotor with a Cable-Suspended Payload," Ph.D. dissertation, Department of Mechanical Engineering and Applied Mechanics, University of Pennsylvania, PA, 2014.
- [2] I. Palunko, P. Cruz, and R. Fierro, "Agile Load Transportation : Safe and Efficient Load Manipulation with Aerial Robots," *IEEE Robotics & Automation Magazine*, vol. 19, no. 3, pp. 69–79, Sept 2012.
- [3] F. A. Goodarzi, "Autonomous Aerial Payload Delivery with Quadrotor using Varying Length Cable," in *Proceedings of the International Conference on Advanced Mechatronic Systems*, Melbourne, Australia, Nov 2016.
- [4] P. Cruz and R. Fierro, "Autonomous Lift of a Cable-suspended Load by an Unmanned Aerial Robot," in *IEEE Conference on Control Applications (CCA)*, Antibes, France, Oct 2014.
- [5] P. J. Cruz and R. Fierro, "Cable-suspended load lifting by a quadrotor UAV: hybrid model, trajectory generation, and control," *Autonomous Robots*, vol. 41, no. 8, pp. 1629–1643, 2017.
- [6] F. A. Goodarzi, D. Lee, and T. Lee, "Geometric control of a quadrotor uav transporting a payload connected via flexible cable," *International Journal of Control, Automation and Systems*, vol. 13, no. 6, pp. 1486–1498, Dec 2015.
- [7] M. M. de Almeida Neto, "Control Strategies of a Tilt-rotor UAV for Load Transportation," Master's thesis, Master Thesis, Universidade Federal De Minas Gerais Escola De Engenharia, Belo Horizonte, Brazil, 2014.
- [8] X. Liang, Y. Fang, N. Sun, and H. Lin, "Dynamics analysis and time-optimal motion planning for unmanned quadrotor transportation systems," *Mechatronics*, vol. 50, pp. 16–29, 2018.
- [9] S. Tang and V. Kumar, "Mixed Integer Quadratic Program trajectory generation for a quadrotor with a cable-suspended payload," in *Proceedings of IEEE International Conference on Robotics and Automation*, Seattle, WA, USA, May 2015.
- [10] P. J. Cruz, M. Oishi, and R. Fierro, "Lift of a Cable-suspended Load by a Quadrotor: A Hybrid System Approach," in *American Control Conference*, Chicago, USA, Jul 2015.
- [11] M. Tognon, C. Gabellieri, L. Pallottino, and A. Franchi, "Cooperative Aerial Transportation without Communication: the Role of Internal Force for Pose Regulation," Laboratoire d'analyse et d'architecture des systèmes, Toulouse, France, Tech. Rep., 2017.
- [12] I. H. Beloti Pizetta, A. Santos Brandao, and M. Sarcinelli-Filho, "Cooperative Quadrotors Carrying a Suspended Load," in *International Conference on Unmanned Aircraft Systems (ICUAS)*, Arlington, VA USA, Jun 2016.
- [13] M. Bernard, K. Kondak, I. Maza, and A. Ollero, "Autonomous Transportation and Deployment with Aerial Robots for Search and Rescue Missions," *Journal of Field Robotics*, vol. 28, no. 6, pp. 914–931, 2011.
- [14] N. Michael, J. Fink, and V. Kumar, "Cooperative manipulation and transportation with aerial robots," *Autonomous Robots*, vol. 30, no. 1, pp. 73–86, 2011.
- [15] P. Kotaru, G. Wu, and K. Sreenath, "Differential-flatness and control of quadrotor(s) with a payload suspended through flexible cable(s)," *arXiv*, 2017.
- [16] T. Lee, "Geometric Control of Quadrotor UAVs Transporting a Cable-Suspended Rigid Body," *IEEE Transactions on Control Systems Technology*. In Press., 2017.
- [17] K. Sreenath and V. Kumar, "Dynamics, Control and Planning for Cooperative Manipulation of Payloads Suspended by Cables from Multiple Quadrotor Robots," in *Conference: Robotics: Science and Systems (RSS)*, Berlin, Germany, Jun 2013.
- [18] I. Maza, K. Kondak, M. Bernard, and A. Ollero, "Multi-uav cooperation and control for load transportation and deployment," *Journal of Intelligent and Robotic Systems*, vol. 57, no. 1-4, pp. 417–449, Jan 2010.
- [19] V. Gavrilets, "Autonomous aerobatic maneuvering of miniature helicopters," Ph.D. dissertation, Massachusetts Institute of Technology, Dept. of Aeronautics and Astronautics, Cambridge, MA, 2003.
- [20] G. Antonelli, F. Arrichiello, and S. Chiaverini, "The null-space-based behavioral control for autonomous robotic systems," *Intelligent Service Robotics*, vol. 1, no. 1, pp. 27–39, 2008.
- [21] L. R. Salinas, E. Slawiński, and V. A. Mut, "Kinematic nonlinear controller for a miniature helicopter via lyapunov techniques," *Asian J. Control*, vol. 16, no. 3, pp. 856–870, 2014.
- [22] D. Gandolfo, L. Salinas, A. Brandão, and M. Toibero, "Path following for unmanned rotorcraft - An approach on energy autonomy improvement," *Information Technology and Control*, vol. 45, no. 1, pp. 87–98, 2016.
- [23] D. C. Gandolfo, L. R. Salinas, A. Brandão, and J. M. Toibero, "Stable path-following control for a quadrotor helicopter considering energy consumption," *IEEE Transactions on Control Systems Technology*, vol. 25, no. 4, pp. 1423–1430, 2017.